Spatial Behaviour of Singularities in Fractal- and Gaussian Speckle Fields

Oleg V. Angelsky[*,1], Alexander P. Maksimyak[1], Peter P. Maksimyak[1] and Steen G. Hanson[2]

[1]*Correlation Optics Dept, Chernivtsi University, 2 Kotsyubinsky Str., Chernivtsi, 58012, Ukraine*

[2]*DTU Fotonik, Department of Photonics Engineering, DK-4000 Roskilde, Denmark*

Abstract: Peculiarities of the spatial behaviour of the dislocation lines resulting from scattering of coherent radiation from random and fractal rough surfaces are studied. The technique of optical correlation is proposed for diagnostics of phase singularities in a complex speckle field by comparing the correlation lengths of amplitude and intensity of the local fields. It is shown that the dislocation lines in the field scattered by a fractal surface have fractal properties, while the dislocation lines scattered off a random surface have no fractal properties.

INTRODUCTION

Scattering of coherent optical radiation by inhomogeneous random objects and media leads to formation of complex spatial distribution of the field due to interference between partial waves with random amplitudes and phases. These intensity distributions are usually referred to as speckle-patterns [1]. The points, where the amplitude of the field equals zero and - as a consequence - the phase is undetermined, will appear at the transversal cross-section of such a field. These points are referred to as phase singularities, amplitude zeroes, or optical vortices. In the vicinity of these points, the wave front is of helicoidal form [2]. The spatial phase singularities form amplitude zero lines or dislocation lines. Please note that the term "zero net" is not true, while these lines do not cross in space, as shown later. The formed skeleton of the electromagnetic field is in general determined by the characteristics of the scattering object and, as so, carries specific information of these objects [3].

Imposing of an off-axis coherent reference wave onto the studied field (the interference technique) is a reliable tool for diagnostics of amplitude zeroes [4-6]. The interference fringes in the vicinity of the amplitude zeros will bifurcate and form so-called interference "forklets" which are easily diagnosed visually. However, detection of amplitude zeroes by the locations of interference forklets in the complex speckle fields is complicated and is hardly automated. Furthermore, the forklet is shifted with respect to the point of zero amplitude by a half period of the interference pattern. Yet, precise location of amplitude zeroes is of high importance for problems of diagnostics of random objects and subsequent reconstruction of their structure. That is why the development of new techniques for locating the phase singularities within fields with the ultimate goal of automating this process and studying the phase singularities becomes an important problem.

In this paper, we recommend the optical correlation technique for diagnostics of amplitude zeroes and for studying

their behaviour in fields scattered by random and fractal rough surfaces.

1. COMPUTER SIMULATION AND COMPUTATION OF THE FIELD

We have carried out computer simulations based on physical modelling of optical fields with phase singularities scattered by a rough surface, which is the most instructive example of light-scattering objects. Two types of surfaces have been modelled, *viz.* random non-fractal (RN) and random fractal (RF) [7-9]. The heights of the inhomogeneities for the random object have been specified by a random generator giving a Gaussian distribution.

Modelling of the fractal surfaces have been performed using the algorithm of successive adding proposed by Voss [10]. Following this algorithm, a surface is formed as the square net with an edge of unitary length and the number of points at the edge equal to $2^n + 1$, where n is the number of steps (cycles) of the modelling procedure. Firstly, one fixes the height at four angles of the net: $h(0,0) = h(0,1) = h(1,0) = h(1,1) = 0$. Then, one uses a subprogram generating independent Gaussian digits ξ with zero mean magnitude and decreasing variance as the number of cycles increase:

$$\sigma_n^2 = (1/\sqrt{2})^{2nH} \sigma_0^2, \qquad (1)$$

where σ_0^2 is the initial variance and H is the Hearst index.

At the initial stage we obtain one magnitude of ξ that is used as the level of surface at the net centre, (1/2, 1/2). The heights at the points with coordinates (0, 1/2), (1/2, 0), (1/2, 1), (1, 1/2), (1/4, 1/4), (3/4, 1/4), (1/4, 3/4) and (3/4, 3/4) are obtained by interpolation, as the arithmetic mean from the heights at the nearest points at the diagonals. Furthermore, 13 independent random numbers $\xi_{n=1}$ with dispersion σ_1^2 are added to the heights, which are present at the mentioned points of the net. This procedure is repeated. The number of repetitions is determined by the desired fractal level. Each cycle of the algorithm doubles the number of points, where

*Address correspondence to this author at the Correlation Optics Dept, Chernivtsi University, 2 Kotsyubinsky Str., Chernivtsi, 58012, Ukraine; E-mail: angelsky@itf.cv.ua

the height is specified diminishing the distance between the points by $1/\sqrt{2}$. The magnitude of the Hearst index is chosen within the interval $0 < H < 1$. RN and RF of sizes 600 x 600 pixels have been computed.

To provide a good approximation between the computer-modelled surface and the real ones, which can be modelled physically, we use the procedure of two-dimensional smoothing of the height inhomogeneities by the Gaussian law with various dispersions.

Relief height probability density function and statistical parameters for random and fractal surfaces are presented in Fig. (**1**) as follows: the arithmetic-mean deviation of the profile from the mean surface line, R_a, root-mean-square deviation, R_q, asymmetry coefficient of the distribution, Sk, and excess coefficient, Ku. This example is with respect to the maximal interval of the surface inhomogeneity heights (the difference between the maximal and minimal heights) $h_{max} = 2\,\mu m$. In the model experiment, h_{max} is changed from $1\,\mu m$ to $100\,\mu m$, which with the given wavelength corresponds to a change of the phase differences from 5 rad to 500 rad.

A rough surface with smooth inhomogeneities can be considered as a phase screen with a phase correlation function $\Psi_\Phi(\rho) = \sigma_{\varphi_0}^2 K(\rho)$, whose maximal magnitude is de-termined by the phase variance of the transparent object, $\sigma_{\varphi_0}^2$, and the lateral behaviour is determined by the correlation coefficient, $K(\rho)$ [11]. The half-width of the correlation function gives the correlation length, l_{φ_0}. The random phase object (RPO) model is based on the following assumptions: the object is infinitely extended and the lateral correlation length of the inhomogeneities is larger than the wavelength, $l_{\varphi_0} > \lambda$.

Infinite extension of the object is provided if all spatial frequencies resulting from light scattered by the probing beam at the object are present in the registration zone. This means that an increase of the object size does not lead to qualitative changes of the field within the registration zone. Of course, the object size must significantly exceed the correlation length of the object phase. So, the registration zone must be within the cone shown in Fig. (**2**), with the base radius $a/2$ and height $z_1 = kal_{\varphi 0}$, which is estimated from the condition of the diffraction minimum. For $a >> l_{\varphi_0}$, the distance z_1 corresponds to the far zone with respect to the isolated inhomogeneity.

The following procedure was implemented for computing the field scattered by a rough surface.

Let us consider a transparent object with a rough surface due to this case being simpler for experimental realization.
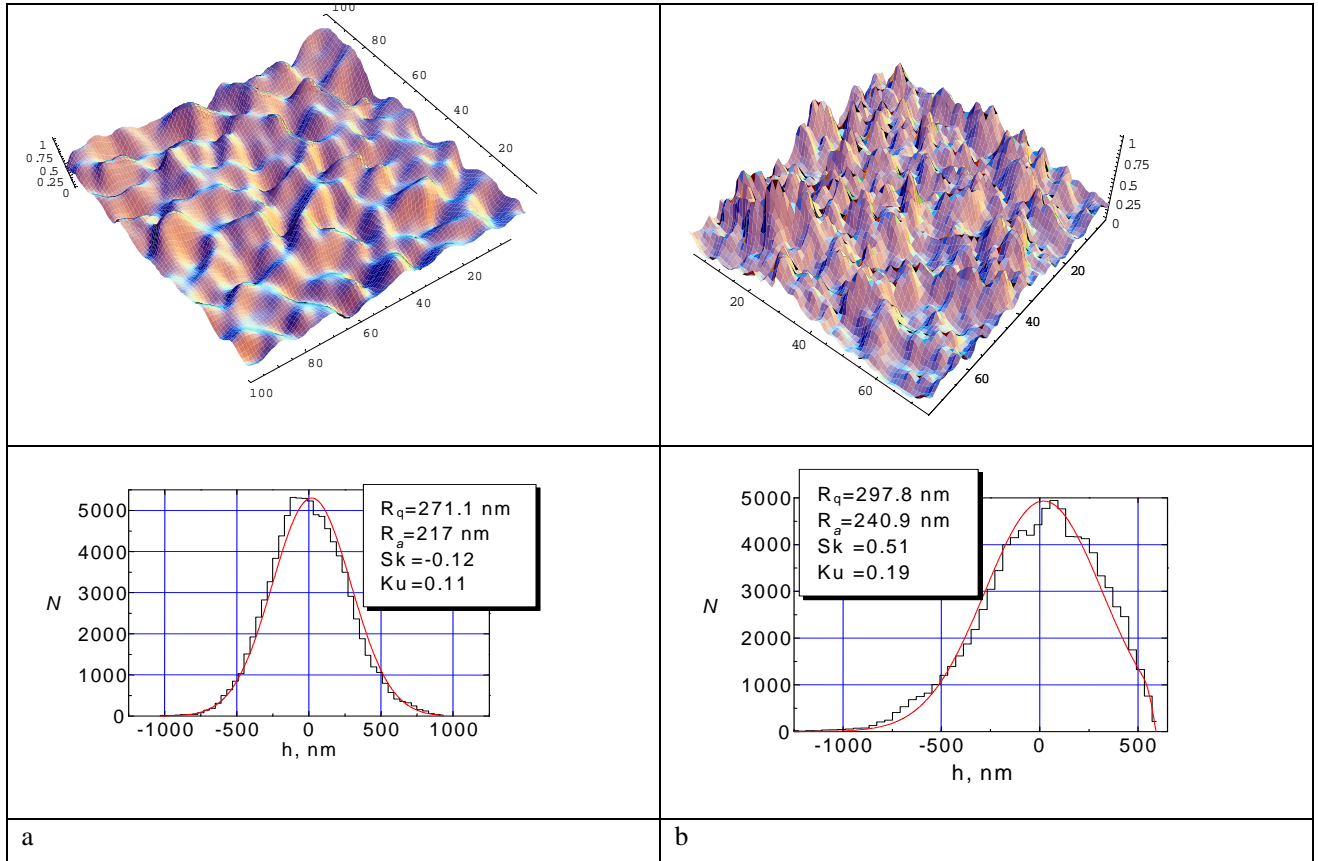

Fig. (1). Relief, height distribution function and statistical parameters of random (**a**) and fractal (**b**) surfaces.

The approach for a reflecting object is the same, the only difference being in the phase delays of the partial beams: $\varphi(x, y) = k(n-1)h(x, y)$ for a transparent object and $\varphi(x, y) = 2k\,h(x, y)$ for a reflected object, where $h(x, y)$ is the relief of the rough surface, n is the refraction index of the object with a rough surface, $k = 2\pi/\lambda$ is the wave number, and λ is the wavelength.
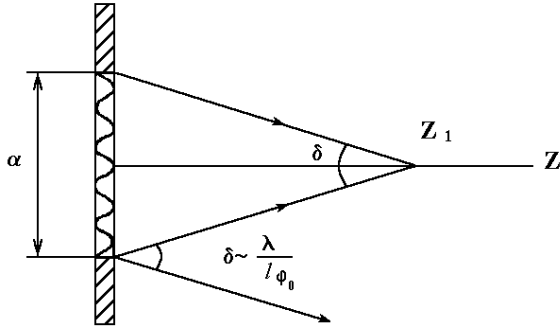

Fig. (2). Estimation of the field registration zone within the framework of the RPS model.

The amplitude and phase distributions of the field resulting from scattering of a plane wave at the phase relief of a rough surface can be found using the double Rayleigh-Sommerfeld diffraction integral [12]:

$$U\left(\xi,\zeta\right) = \frac{z}{i\lambda} \int\int \frac{F\left(x, y\right)}{R^2\left(x, y, z, \xi, \zeta\right)} \cdot$$
$$\exp\left\{-ik\left[R(x, y, z, \xi, \zeta) + (n-1)h(x, y)\right]\right\}dxdy \tag{2}$$

where $F(x, y)$ is the aperture function corresponding to the amplitude transmittance of a rough surface; $R(x, y, z, \xi, \zeta) = \sqrt{z^2 + \left(x - \xi\right)^2 + (y - \zeta)^2}$ is the distance from the object point to the point at the observation plane; z is the distance between the surface plane and the observation plane; x, y and ξ, ζ are the Cartesian coordinates at the object plane and at the observation plane, respectively (cf. Fig. **3**).
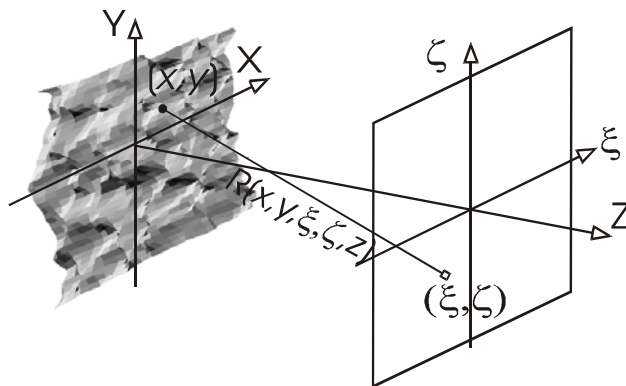

Fig. (3). Formation of the field scattered from a rough surface.

The integral (2) can be used for computation of the field at arbitrary distances from the object to the observation plane [12].

In this study, we replace integration by summation, and divide the object and the observation plane in elementary cells. For obtaining reliable results, the distance between the points in which the object is divided must be less than $\lambda/2$. Computing the field of the scattered radiation $U(\xi, \zeta)$, we find its real and imaginary parts, $\mathrm{Re}\,U(\xi, \zeta)$ and $\mathrm{Im}\,U(\xi, \zeta)$. The complex amplitude of the field, $U(\xi, \zeta)$, the modulus of amplitude, $A(\xi, \zeta)$, the phase, $\varphi(\xi, \zeta)$, and intensity of the resulting field, $I(\xi, \zeta)$, are determined from the following equations:

$$U(\xi, \zeta) = \mathrm{Re}\left[U(\xi, \zeta)\right] + i\,\mathrm{Im}\left[U(\xi, \zeta)\right], \tag{3}$$

$$A((\xi, \zeta)) = \sqrt{\mathrm{Re}\left[U(\xi, \zeta)\right]^2 + \mathrm{Im}\left[U(\xi, \zeta)\right]^2}, \tag{4}$$

$$\varphi(\xi, \zeta) = \mathrm{arctg}\left[\frac{\mathrm{Im}\,U(\xi, \zeta)}{\mathrm{Re}\,U(\xi, \zeta)}\right], \tag{5}$$

$$I(\xi, \zeta) = \mathrm{Re}\left[U(\xi, \zeta)\right]^2 + \mathrm{Im}\left[U(\xi, \zeta)\right]^2. \tag{6}$$

2. BEHAVIOUR OF THE DISLOCATION LINES IN THE OPTICAL FIELD

An example of the field scattered from a rough surface in the far zone with respect to the typical isolated inhomogeneity is shown in Fig. (**4**). The experimental parameters were: $h_{max} = 8$ μm; object size – 400x400 μm; the number of pixels in the object – 1200x1200; the field size – 5x5 μm; the number of pixels in the field – 1000 x 1000; z=100 μm. One can see from the phase distribution of the field (Fig. **4b**) that phase singularities are present in the field. These singularities are at the ends of the lines of phase discontinuities. Fig. (**4c**) also shows the lines $\mathrm{Re}[U], \mathrm{Im}[U] = 0$ (green and yellow) whose crossings determine the coordinates of the phase singularities [2, 4, 13].

It is traditionally supposed that the lines of the phase singularities are closed-loops, i.e. pairs of singularities arise and annihilate [14-16]. In practice it is not always so. In part, it has been shown [17, 18] that the dislocation lines in three-dimensional space often form knotted and linked phase singularities.

To study the behaviour of the phase singularity lines for optical fields, we have developed dedicated computational software. To develop the algorithm for determination of the phase singularity coordinates, we use the fact that both the real and imaginary parts of the complex amplitude must change sign from one pixel to the next. Obtaining in such a manner the pixel coordinates we compute the field in some vicinity ΔL of this point changing the distance from the object Z with some step Δz. Furthermore, we determine the coordinates of an amplitude zero for the obtained field amplitude distribution. If a phase singularity is absent for this distribution, one returns to the previous step, doubles the
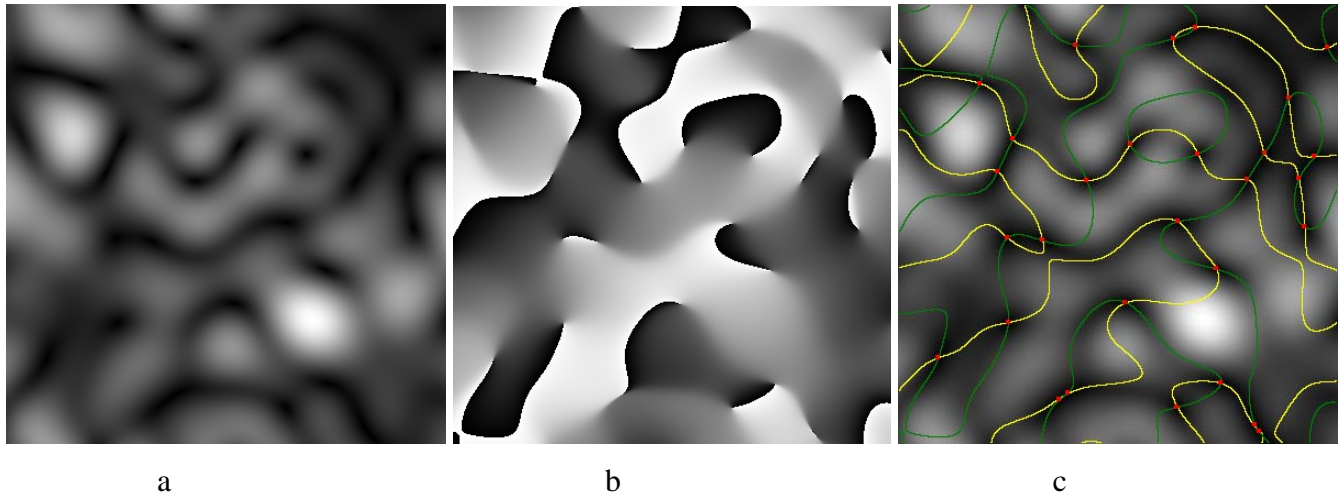
<center>a   b   c</center>

Fig. (4). Example of the field scattered off a rough surface: intensity distribution (**a**), phase distribution (**b**); the lines $\mathrm{Re}[U], \mathrm{Im}[U] = 0$, whose crossings determine the coordinates of the phase singularities (**c**).

observation area and determines the coordinates of another singularity that apparently annihilated with the first singularity. Subsequently, the position of the second singularity is searched for in the opposite direction.

An example of a set of line phase singularities forming the skeleton of a field scattered from the same surface is shown in Fig. (**5**). Points at the singularity lines are determined with an interval of 20 nm along the *z*-axis. To improve transparency, the planes separated with steps of 2 µm are drawn in Fig. (**5**). Crossing of the dislocation lines with each plane are shown by points of the same colour.
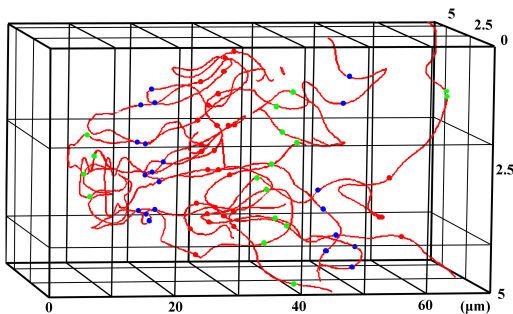

Fig. (5). Example of the set of line phase singularities forming the skeleton of a field scattered at a rough surface.

It can be seen from Fig. (**5**) that the phase singularities appear at the boundary field. Formation of two vortices of opposite signs is not accompanied, as a rule, by annihilation, while the probability of this process is very low, though a few closed lines are not excluded [18]. Discontinuities of the skeleton lines are absent within the considered region of the field, which is seen in the corresponding animation (avi 1). Line discontinuities are observed only at the output of the considered region. Thus, the phase dislocation skeleton of the scattered radiation field is a continuous line within the investigated region extending both in longitudinal and in transverse directions.

An example of a fragment of such line for the fractal rough surface is shown in Fig. (**6**). The experimental parameters are: $h_{max} = 8$ µm; object size – 400x400 µm; the number of pixels in the object – 1200x1200; size of the field – 5x5 µm, the number of pixels in the field – 1000x1000. One can track the course of this line in the volume in the animation (avi 2).
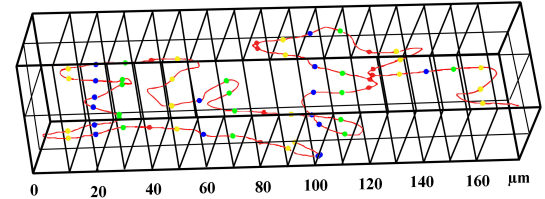

Fig. (6). Example of the fragment of the phase singularity skeleton for the field scattered by a fractal object.

We have analyzed the behaviour of the dislocation lines for fields scattered by random and fractal rough surfaces. It has been found that the dislocation lines for fractal rough surfaces have fractal properties, while such properties are absent in the case of random rough surface, as will be discussed next. The fragments of the dependencies of the transverse shift of the phase dislocation line for passing this line along the *z*-axis with step size Δz for the fields scattered at random and fractal objects are shown in Fig. (**7**), fragments (**a**) and (**b**), respectively.

The power spectra for the dependency of the transversal shift of the phase dislocation line for passing this line along *z*-axis with the step size Δz for fields scattered by random and fractal objects are shown in Fig. (**8**), fragments (**a**) and (**b**), respectively.

One can ascertain the signatures of fractal behaviour of the dislocation line for the field scattered by the fractal surface. This is clearly seen from the behaviour of the log-log dependence (Fig. **8a**), where the envelope of the power spectrum is almost a straight line.
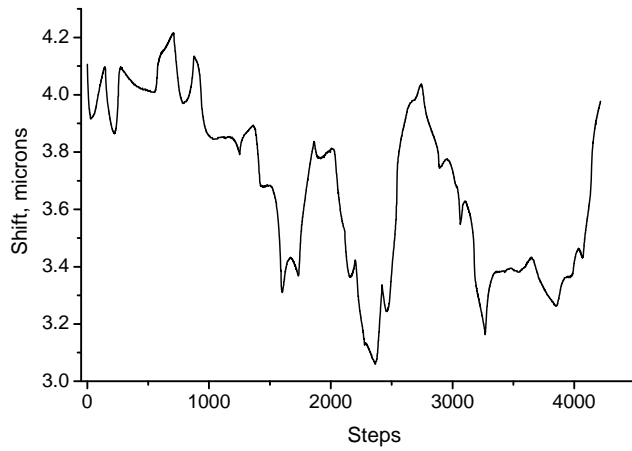
a
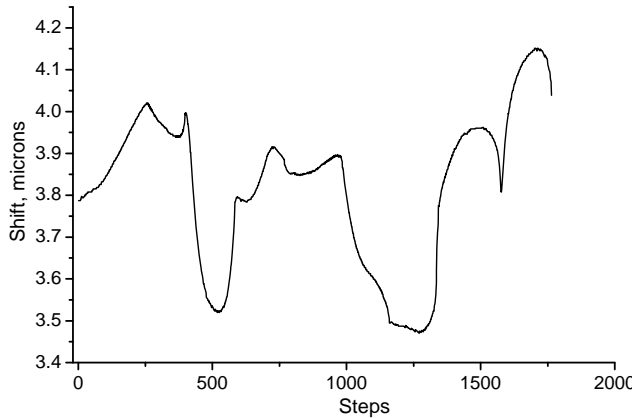
b

Fig. (7). Fragments of the dependencies of the transversal shift of the phase dislocation line for passing this line along *z*-axis with steps Δz for the fields scattered off fractal (**a**) and random (**b**) objects.

It has been shown [19] that the power spectrum for the fractal curve can be represented in the following form:

$$S(f) = k / f^{\alpha} = kf^{-2H-1}. \tag{7}$$

On the other hand, following Mandelbrot [20], the fractal dimension of a two-dimensional surface fractal (curve) is determined based on the Hearst index *H* determining the double slope of the logarithmic dependence of the structure function in the following manner:

$$D_f = 2 - H. \tag{8}$$

The logarithmic dependency of the power spectrum $S(f)$ is straight only for the curve corresponding to the fractal object (Fig. **8**). The magnitude of the fractal dimension for the specific fractal curve in Fig. (**7a**) is $D_f = 1.52$. The fractal dimension for the phase singularity lines for various heights of inhomogeneities is shown in Fig. (**9**). One observes an increase of the fractal dimension saturated at the level $D_f = 1.62$.
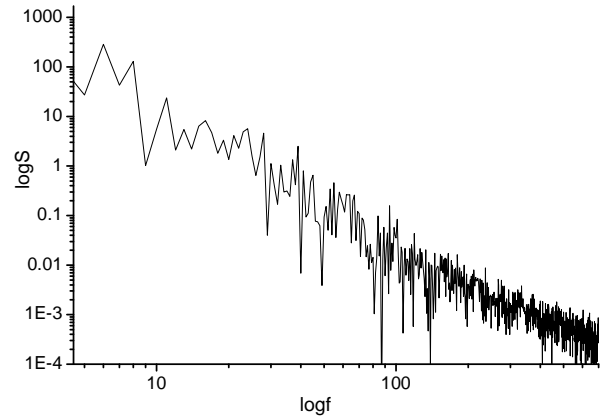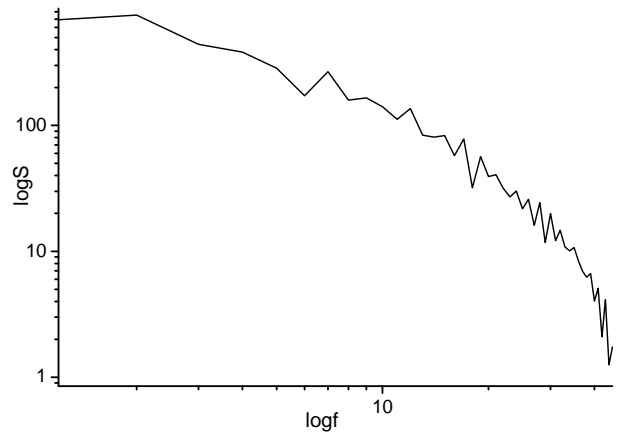
Fig. (8). Power spectra for the dependencies of the transversal shift of the phase dislocation line for passing this line along *z*-axis with step size Δz for the fields scattered off fractal (**a**) and random (**b**) objects.
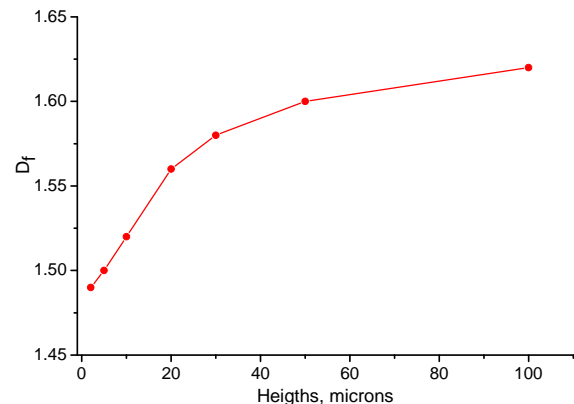

Fig. (9). Dependency of the fractal dimension for the phase singularity lines for various heights of the inhomogeneities of the fractal object.

The behaviour of the fractal dimension of the phase singularity lines can be described within the framework of the notions of the generalized Brownian motion. The phase singularity lines for small height intervals of the fractal surface correspond to the classical Brownian motion (H =0.5). Increasing the height interval leads to larger phase delays between the scattered waves and, as a consequence, to stronger chaostization of the phase fluctuations. This results in a decrease of the Hearst index $H < 0.5$ and, correspondingly, in an increase of the fractal dimension $D_f > 1.5$.

Thus, the phase singularity lines for a random field are continuous complex lines extending both in longitudinal and in transverse directions. The phase singularity lines for the field scattered by fractal surfaces possess fractal properties, while such properties are absent for scattering off non-fractal surfaces.

3. DETERMINATION OF COORDINATES OF AMPLITUDE ZEROES AT MONOCHROMATIC SPECKLE FIELD

At the centre of the optical vortex, the intensity vanishes. That is why it seems that measuring of the field intensity is a simple and reliable technique for determination of the exact vortex coordinates. However, such measurements are not unambiguous, since the field contains points where the intensity approaches zero but the phase does not comprise a singularity, cf. the intensity distribution $I(x, y)$ in Fig. (**10a**). Experimental discrimination of such points based on the points of zero amplitude is difficult. For example, the coordinate distribution of the intensity minima for the field represented in Fig. (**10a**) is shown in Fig. (**10b**).

Analyzing the phase distribution of this field, $\Phi(x, y)$, (Fig. **10c**) one can see that the number of intensity minima is larger (13) than the number of singular points (9).
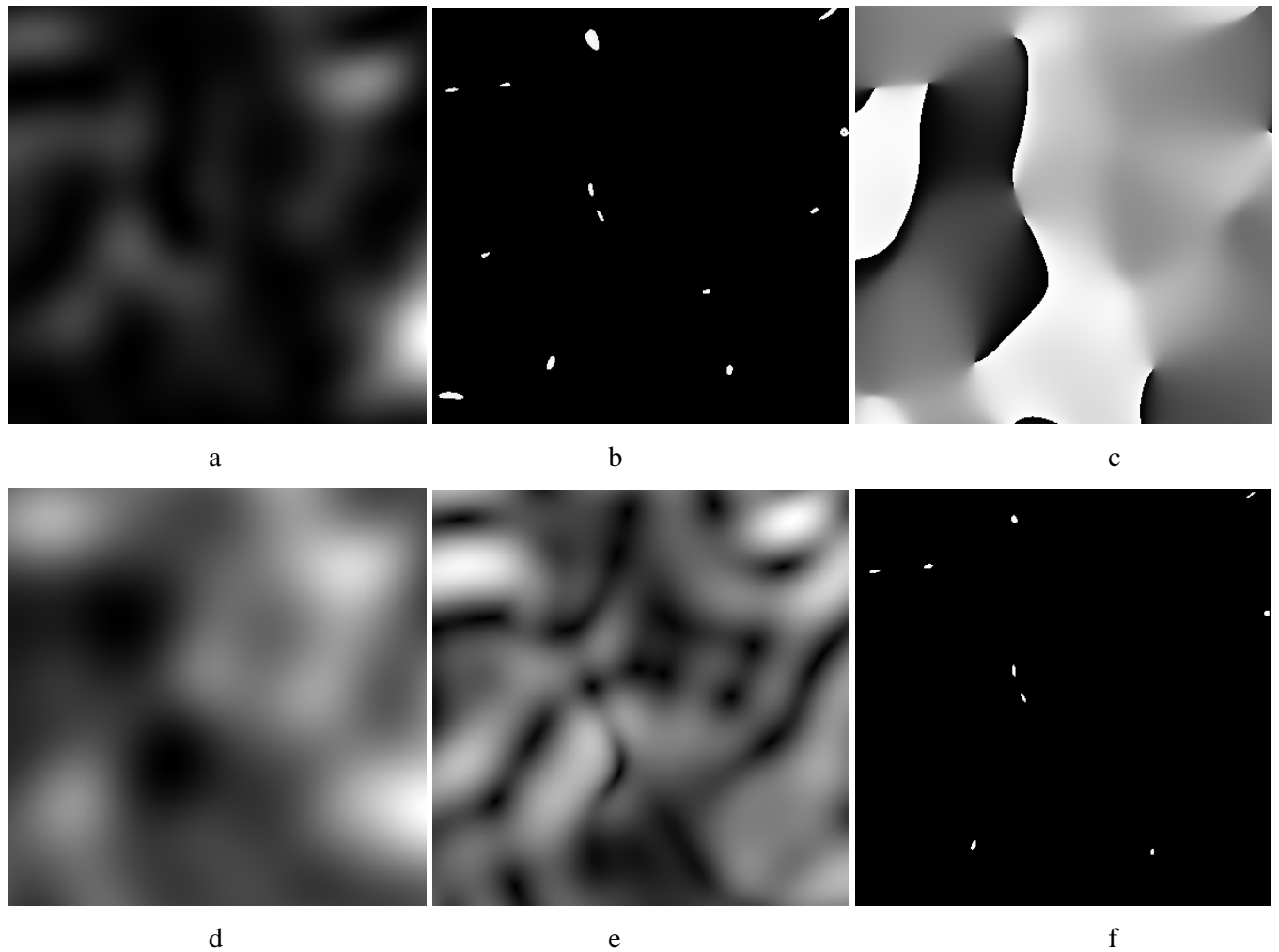

a   b   c

d   e   f

Fig. (10). Distributions of the parameters of the field scattered at a rough surface: intensity distribution $I(x, y)$ (**a**); coordinate distribution of intensity minima (**b**); phase distribution $\Phi(x, y)$ (**c**); intensity distribution of the resulting field $U(x, y) + U_0$ (**d**); distribution of the intensity gradient modulus of the resulting field $\left|\nabla\left|U(x, y) + U_0\right|^2\right|$ (**e**); coordinate distribution of the phase singularities $S(x, y)$ (**f**).
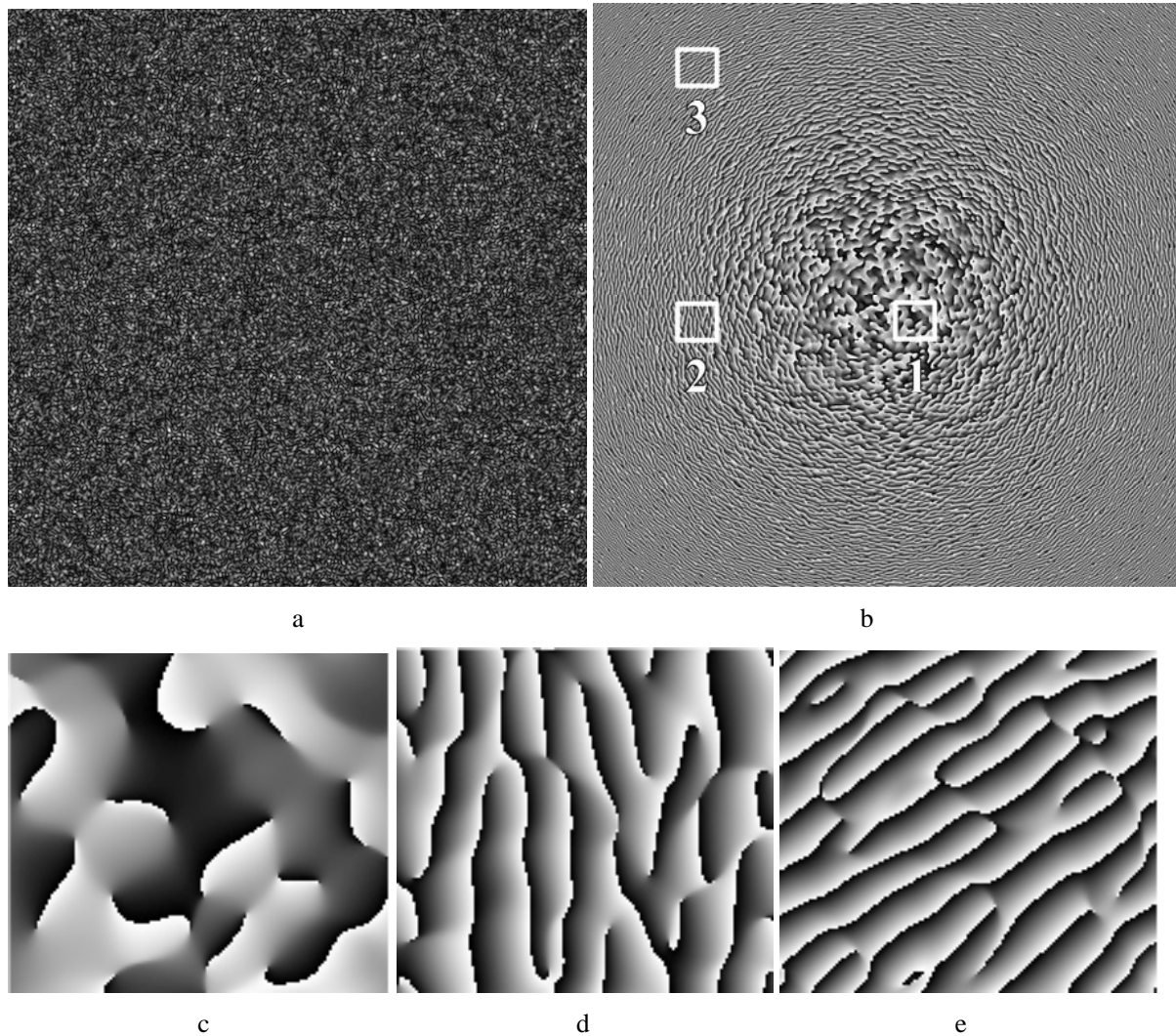
Fig. (11). Intensity distribution of the field (**a**), phase distribution (**b**), and the magnified areas 1-3 of the phase distribution (**c-e**).

For determination of the amplitude zero coordinates we impose a strictly coaxial reference wave U_0 to the optical field $U(x,y)$ (Fig. **10d**). The phase delay between the fields in this case can be arbitrary. As a result, non-zero gradient of intensity arises at the amplitude zero points; while the intensity gradient at the intensity minima points without a phase singularity is in practice zero (Fig. **10e**). For pixel-by-pixel division of the distribution of the resulting field gradient by the intensity of the input field one obtains the maximal magnitudes of the distribution:

$$F(x,y) = \frac{\left| \nabla \left| U(x,y) + U_0 \right|^2 \right|}{I(x,y)}.$$

Normalizing this function by its maximal value,

$$F^n(x,y) = \frac{F(x,y)}{F_{max}},$$

and using the condition

$$S(x,y) = \begin{cases} 1, (F(x,y) + \delta \geq 1) \\ 0, (F(x,y) + \delta < 1) \end{cases}$$

highlights the coordinate distribution of amplitude zeroes (Fig. **10f**), which strictly coincides with the amplitude zero distribution obtained from the phase distribution in Fig. (**10c**). Here δ is the experimental noise of the CCD-camera or the computing errors during computer simulation. Increasing δ results in increasing the area within which the coordinates of the amplitude zeroes lie.

4. RECOGNITION OF STRONGLY SCATTERING OBJECTS

The above technique for diagnostics of amplitude zeroes is applicable for the model based on infinite random phase object as well, especially relevant in the case with a limiting aperture.

Determining the coordinate distribution of phase singularities is useful in connection with the problem of strongly scattering objects. So, in the intensity distribution of a field (size 3x3 mm^2) scattered by a strongly rough surface (size 1x1 mm^2) and registered at a distance of 40 mm from the

object within its geometrical shadow, the contours of the objects are not visualized (Fig. **11a**). But the phase distribution of the field contains such information, as it is seen from Fig. (**11b**). A detailed analysis of the phase distribution leads to the conclusion that the density of amplitude zeroes for various areas of the field is approximately constant, though the curvature of the averaged phase front increases for areas at larger distances from the central part of the field (Fig. **11c-e**).

It has been shown [21] that a plane reference wave coaxially imposed onto such field causes a non-uniform spatial-frequency distribution of the intensity. Holographic registration of objects placed at a large distance has previously been considered [22]. Due to interference addition of various spatial-frequency components of the scattered field with the reference wave, the period of modulation within the geometrical shadow of the object is two times larger than the period at the edges, which results in reconstruction of the object macro-form contoured by speckles of smaller dimensions. The object is recognized up to an angular size ~0.05 rad. For local measurements of the period of an interference pattern, the computer software for processing of an interference pattern is needed, but implementation of such software for complex and volume objects is difficult.

We have now established that the distribution of the density of amplitude zeros for the field with a coaxially imposed plane reference wave provides visual information on the object contours. The intensity- and phase distributions in case the intensity of the reference wave equals the average intensity of the object field are shown in Fig. (**12a, b**), respectively. One observes spatially non-uniform modulation of the distributions of intensity and phase of the resulting field with a radially decreasing period. This is caused by interference between various spatial-frequency components of the scattered field with the reference wave. The phase distributions of the resulting field for various areas are shown in Fig. (**12c-e**). The amplitude zeroes are localized at the ends of the lines of a phase discontinuity.

The density of amplitude zeroes increases for areas away from the central part of the field. As a result, the macro-form of the studied object manifests itself (Fig. **13**).

This fact can be illustrated for the model experiment, the results of which are represented in Fig. (**14**), where intensity- and phase distributions are shown. The reference wave is imposed onto the area of an optical field with a single phase singularity (Fig. **14a**) under various angles φ with respect to the direction of propagation of the illuminated wave. The angle φ is changed from 0.02 rad to 0.2 rad. Increasing the angle φ results in a decrease of the period of the interference pattern and increasing of the number of amplitude zeroes for the resulting field, as it is seen in Fig. (**14b-e**).
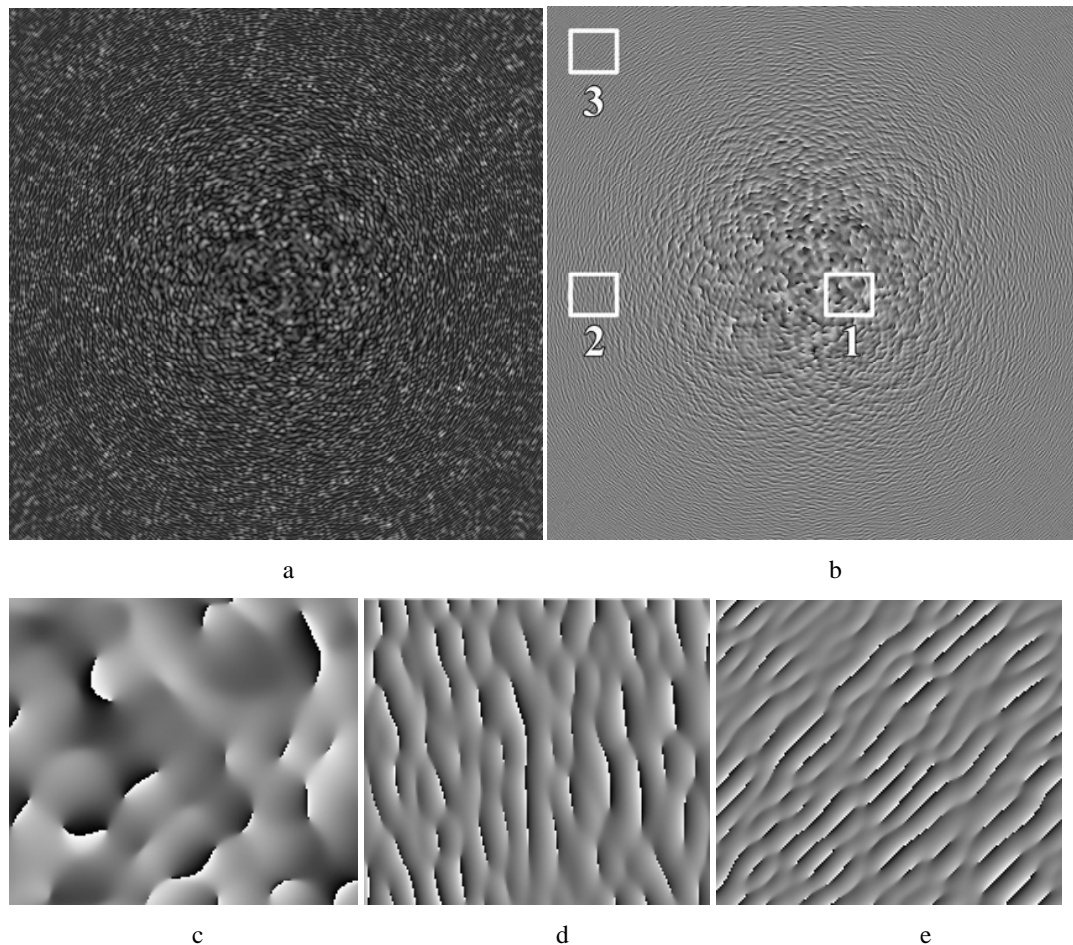

a   b

c   d   e

Fig. (12). Intensity distribution of the field with a reference wave (**a**), phase distribution (**b**), and magnified areas 1-3 of the phase distribution (**c-e**).

Thus, the coordinate distribution of the phase singularities in the field with coaxially imposed reference wave provides visualization of strongly scattering objects.
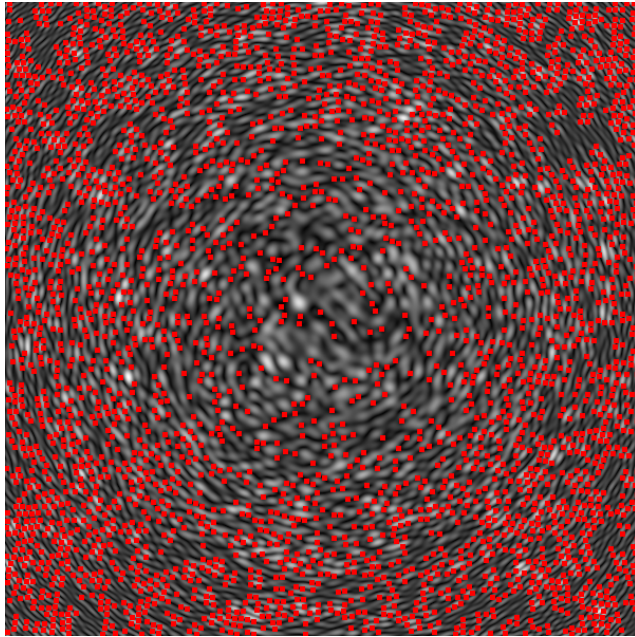

Fig. (13). Amplitude zero distribution.

5. INVESTIGATION OF THE DEPENDENCE OF THE NUMBER OF AMPLITUDE ZEROS IN FIELDS SCATTERED FROM SURFACES WITH VARYING SURFACE ROUGHNESS

In the field scattered from a rough surface with limited irradiance width, the average number of amplitude zeroes must decrease for increasing distance from the object to the observation plane due to the spatial-frequency filtering. But we assume that a rough surface is an infinitely extended RPO. Let us consider the dependence of the number of amplitude zeroes in a field scattered from a rough surface dependent on the position of the registration zone and dependent on the maximal interval of heights, all within the framework of the RPO model. Computer simulation of light scattering of monochromatic radiation has been performed for a surface with a Gaussian height distribution and with the following parameters for the experiment: object size – 400x400 μm, the number of pixels in the object – 1200x1200, field size – 10x10 μm, the number of pixels in the field – 1000x1000 [7-9].

The coordinates of phase singularities are determined by the crossing of the lines $\mathrm{Re}[U], \mathrm{Im}[U] = 0$ (green and yellow, respectively) (Fig. **4c**). Subsequently, the total number of phase singularities in the analyzed field is counted. The functional dependence between the surface roughness and the number of singularities are shown in Fig. (**15**). These dependencies have two maxima for the maximal interval of heights from 2 to 20 μm. The first maximum is at the focusing zone, and the second one is at the beginning of the Fraunhofer with respect to the isolated inhomogeneity zone. So, for surfaces with the intervals of heights 2, 5, 10 and 20 μm we obtain the position of the first maximum at the distances from the surface at 200, 80, 40 and 15 μm, respectively.

The first maximum is absent for the heights of surface inhomogeneities from 30 to 100 μm, where both the focusing zone and the Fraunhofer zone are very close to the object and thus are not well separated. Therefore, as the interval of heights of surface inhomogeneities increases, the maximum number of phase singularities in the field is saturated and reaches an approximate magnitude of 450 for the specified size of the area of analysis, here 10x10 μm.
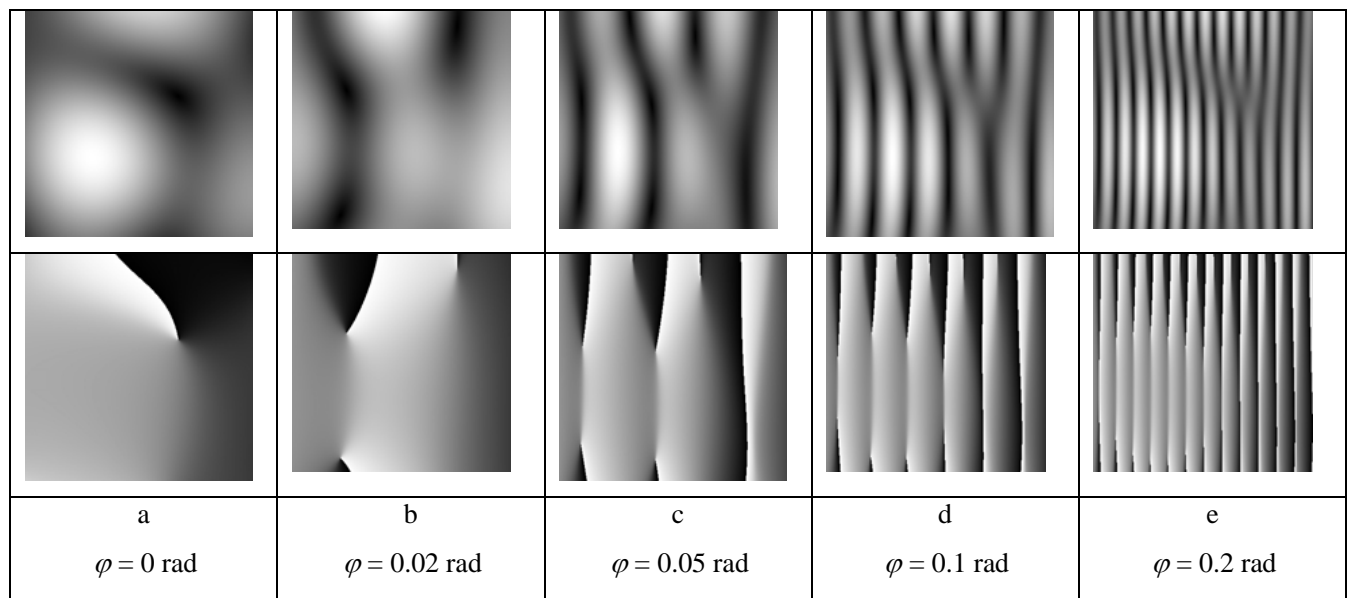

a	b	c	d	e
$\varphi = 0$ rad	$\varphi = 0.02$ rad	$\varphi = 0.05$ rad	$\varphi = 0.1$ rad	$\varphi = 0.2$ rad

Fig. (14). The model experiment in which a reference wave is imposed onto the area of an optical field with a single phase singularity (**a**) under angles φ : 0.02 (**b**); 0.05 (**c**); 0.1 (**d**) and 0.2 rad (**e**). Upper and lower rows show intensity- and phase distributions, respectively.

The maximum number of amplitude zeroes in the scattered field as a function of the heights of the inhomogeneities for a rough surface depends on the size of the registration zone and may be approximated by the following empirical formula:

$$N_{max} = 4L^2(1 - \exp(-\sigma_h / \pi))^2 / \pi e \lambda^2 , \qquad (9)$$

where L is the field size; e is the Euler number; σ_h is the dispersion of heights of surface inhomogeneities (root-mean-square deviation of a profile from a mean surface line), which equals $h_{max} / 4$.
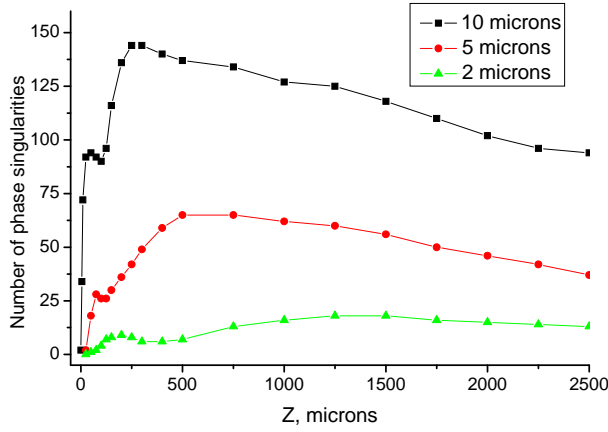
a
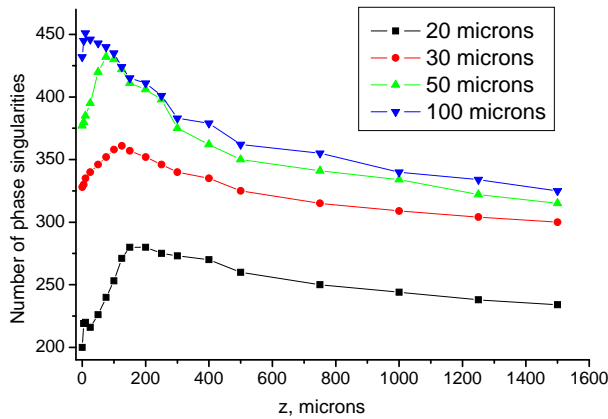
b

Fig. (15). The number of phase singularities in the registration zone as a function of the distance from the surface for the surface roughness 2-10 μm (**a**) and 20-100 μm (**b**).

The results of computer simulation compared with the above approximation for the maximum number of phase singularities in the scattered field from a rough surface is shown in Fig. (**16**). Thus, one can determine the root-mean-square roughness of a surface by measuring the maximum number of phase singularities in the scattered field and using Eq. (9).

6. INVESTIGATION OF THE BEHAVIOUR OF PHASE SINGULARITIES BY MEASURING THE CORRELATION FUNCTION OF A FIELD

The transverse correlation functions of the field and of the intensity for an optical field with phase singularities are different from each other with respect to the transverse scale. The correlation length of the field in this case is larger than the correlation length of the intensity. These correlation lengths are equal to each other in fields without phase singularities.
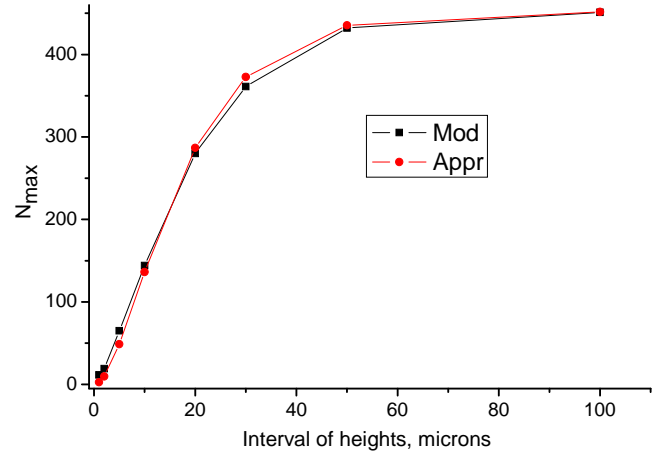

Fig. (16). Simulated dependency of the maximum number of phase singularities in the field for varying heights of surface inhomogenities (Mod) and the approximating curve (Appr).

Let us write the correlation function for the field in the form [12]:

$$\Psi_\perp\left(\vec{\rho}, z\right) = \left\langle \tilde{u}\left(\vec{\rho}_1, z\right) \tilde{u}^*\left(\vec{\rho}_2, z\right) \right\rangle .$$

The intensity correlation function is of the form:

$$\Psi_I\left(\vec{\rho}, z\right) = \left\langle \tilde{I}\left(\vec{\rho}_1, z\right) \tilde{I}\left(\vec{\rho}_2, z\right) \right\rangle ,$$

where $\vec{\rho} \equiv \vec{\rho}_1 - \vec{\rho}_2$ is based on the assumption of stationarity. The normalized correlation functions for field and intensity are given by the correlation coefficients, $K_\perp(\vec{\rho}, z)$ and $K_I(\vec{\rho}, z)$, respectively, the use of which provides the possibility to compare the transverse scales of fields.

We have developed a program for computing the transverse correlation function of intensity and the transverse coherence function of a field. The computing procedure consists of:

A. Determination of the Correlation Length of the Intensity

One forms a two-dimensional matrix I, the elements of which correspond to the intensity of a field at specified spatial positions. Further, shifting this matrix with respect to itself in the transverse direction at some number of steps l, one obtains the correlation function:

$$F_{cor}\left(l\right) = \frac{\sum_{i,j}\left(I_{i,j} \times I_{i+l,j}\right)}{\sum_{i,j}I_{i,j} \times \sum_{i,j}I_{i+l,j}} .$$

Then, one finds the shift l_0 for which $F_{cor}\left(l_0\right) > 0.5$ giving the half-width of the correlation function, i.e. the correlation length of the field intensity:

$$R_{cor} = \left| \frac{k - \dfrac{0.5 - F_{cor}\left(l\right)}{F_{cor}\left(l-1\right) - 0.5}}{1 + \dfrac{0.5 - F_{cor}\left(l\right)}{F_{cor}\left(l-1\right) - 0.5}} \right| .$$

B. Determination of the Field's Correlation Length

One separately adds and subtracts the real and imaginary parts of the complex amplitude of a field forming the intensity extrema $I_{max}\left(l\right)$ and $I_{min}\left(l\right)$ for shift l, respectively:

$$I_{min}\left(l\right) = \sum_{i,j}\left(\left(U_{i,j}^{re} - U_{i+l,j}^{re}\right)^2 + \left(U_{i,j}^{im} - U_{i+l,j}^{im}\right)^2\right),$$

$$I_{max}\left(l\right) = \sum_{i,j}\left(\left(U_{i,j}^{re} + U_{i+l,j}^{re}\right)^2 + \left(U_{i,j}^{im} + U_{i+l,j}^{im}\right)^2\right).$$

Further, one obtains the coherence function by dividing difference of the intensity extrema $I_{max}\left(l\right)$, $I_{min}\left(l\right)$ by their sum:

$$F_{coh}\left(l\right) = \frac{I_{max}\left(l\right) - I_{min}\left(l\right)}{I_{max}\left(l\right) + I_{min}\left(l\right)} .$$

One finds the step k_1 for which $F_{coh}(k_1) > 0.5$ and determines the half-width of the correlation function:

$$R_{coh} = \left| \frac{l - \dfrac{0.5 - F_{coh}\left(l\right)}{F_{coh}\left(l-1\right) - 0.5}}{1 + \dfrac{0.5 - F_{coh}\left(l\right)}{F_{coh}\left(l-1\right) - 0.5}} \right| .$$

Study of the dependence of the correlation lengths of the field and its intensity in the observation plane has been performed for random and fractal surfaces.

The field and intensity correlation coefficients for scattering from a random rough surface with the interval of heights 20 μm observed at a distance of 100 μm from an object are presented in Fig. (**17**).

One observes considerable difference between the correlation lengths: $0.206\,\mu m$ and $0.302\,\mu m$. Thus, the ratio of the correlation lengths of intensity and field, $a = l_I/l_\perp$, can be considered as the criteria of the presence of amplitude zeroes for the optical field: if $a < 1$, then zero amplitudes are present in the field.

The dependencies of the correlation lengths for intensity, l_I, and for a field, $l_\perp$, as well as their ratio a are presented in Fig. (**18**), as function of the distance between the object and the observation plane. These correlation lengths are equal to each other at the boundary object field. As the distance from the object to the observation plane increases, the field correlation length is almost unchanged, while the intensity correlation length rapidly decreases at the focusing zone and reaches a stable magnitude at the Fraunhofer zone. Note, for $z > 150$ μm both correlation lengths increase due to spatial-frequency filtering, and their ratio is approximately constant.

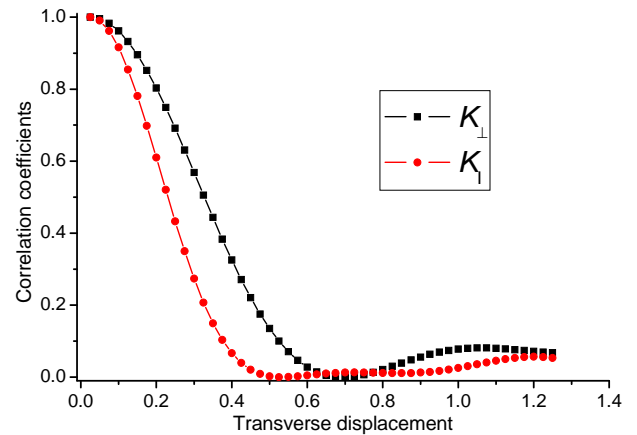**Fig. (17).** Field $K_\perp(\vec{\rho}, z)$ and intensity $K_I(\vec{\rho}, z)$ correlation coefficients of a field scattered from a random rough surface with the interval of heights 20 ì m and probed at a distance of 100 ì m from the object.
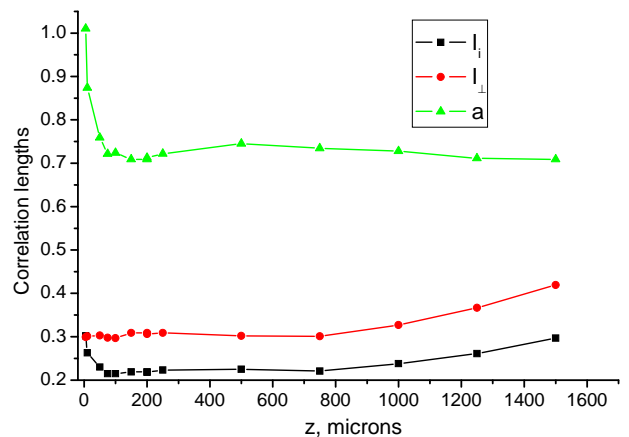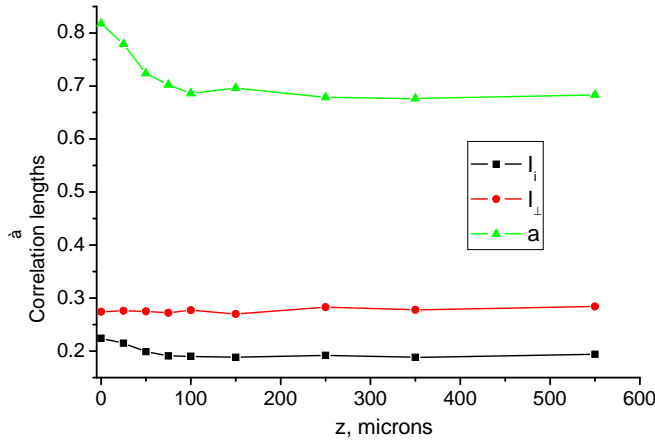

Fig. (18). Dependencies of the correlation lengths of intensity, l_I, and of a field, $l_\perp$, and their ratio, a, on the distance to the registration zone for a field scattered at random rough surface with the interval of heights 20 μm.

For larger intervals of heights for a rough surface, the behaviour of the correlation lengths of the scattered field is similar (Fig. **19**).

For a fractal surface, the ratio of the correlation lengths $a = l_I/l_\perp$ approximately stays constant as the distance from

an object to the registration plane increases (Fig. **20**). The correlation lengths increase much more monotonically with no extrema. This is explained by the absence of a clearly pronounced focusing zone in the field scattered from a fractal rough surface.

In practice, the ratio of the correlation lengths is saturated in the far field at the level 0.66-0.70 for all intervals of heights of a rough surface. This means that the use of the ratio of the correlation lengths with diagnostic purposes is not convenient. However, knowing the field correlation length, one can estimate the number of speckles (inhomogeneities of intensity) and number of inhomogeneities of a field for various zones of registrations.

a
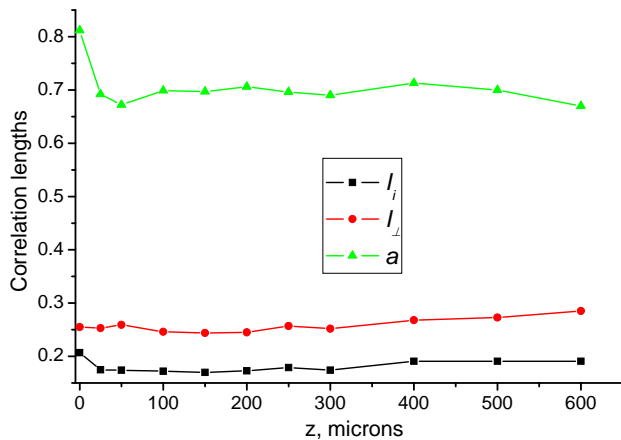
b

Fig. (19). Dependencies of the correlation lengths of intensity, l_I, and field, $l_\perp$, and their ratio, a, on the registration zone for a field scattered from a random rough surface with the intervals of heights 30 μm (**a**) and 50 μm (**b**).

Obviously, the number of amplitude zeroes and the number of speckles in the field are interconnected. It is believed that in a random field the number of speckles equals the number of phase singularities [4, 5]. We will consider the correlation between the number of speckles and the number of phase singularities in a field scattered from a rough sur-

face in more details, within the framework of the RPO model.

Generally, the number of speckles in a field attains its maximum when the speckle size is minimum, i.e. in the case when speckles are formed by the oppositely directed beams. In this case, the size of a speckle does not exceed $\lambda/2$. For $\lambda = .6328\mu$m the smallest speckle size is $\rho = 0.315\mu$m. To count the number of speckles, one must fill the observation area with speckles. The densest filling takes place in the case when the contours of speckles are of hexagonal form. In this case, an area of the field $\rho^2\sqrt{3}/2$ corresponds to the speckle with area $\pi\rho^2/4$, and the ratio of these areas determines the coefficient of filling of the area of observation by speckles.
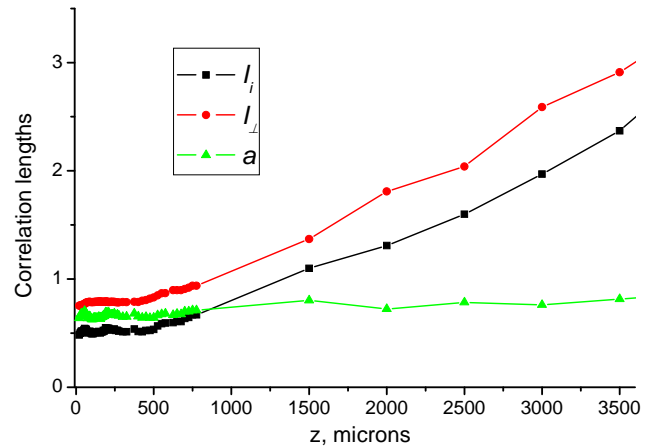

Fig. (20). Dependencies of the correlation lengths for intensity, l_I, and for the field, $l_\perp$, and their ratio, a, as a function of the distance to the registration zone for a field scattered at fractal rough surface with the intervals of heights 20 μm.

The maximum number of speckles, N_{max}, that can be placed in the area of the field S, 10x10 μm^2 is determined by the ratio

$$N_{max} = \frac{c \cdot S}{s_{min}},$$

where c is the coefficient of filling of an area by speckles, s_{min} is the minimum area of a speckle, and this number will equal 1155.

Computer simulation of scattering of optical radiation from a rough surface gives the maximum number of speckles for the interval of heights if inhomogeneities of a rough surface 100 μm (when one already observes saturation of the dependence of the number of speckles on the interval of heights of inhomogeneities) equal to 452. This number of speckles is much smaller than predicted by theory, even for the highest density of speckles. This is connected with the fact that the role of low spatial frequencies in formation of a speckle field is much larger than the role of high spatial frequencies, while the intensity of a field is proportional to

$1/R^2$, where R is the distance from an object point to the point of observation.

Fig. (**21**) shows the number of computed amplitude zeroes in the observation plane for a size of $40\text{x}40\,\mu\text{m}^2$. The correlation length of the scattered intensity is $2\mu\text{m}$.

In the far field with respect to an isolated inhomogeneity of a rough surface one observes almost twice the number of amplitude zeroes than the number of computed speckles. Such a correlation of the number of speckles and the numbers of amplitude zeroes is possible in the case of hexagonal form of speckles. Though, as the registration zone is further displaced from the object, both the number of speckles and the number of amplitude zeros decrease, so that in the far field with respect to the entire object, these numbers approach each other.
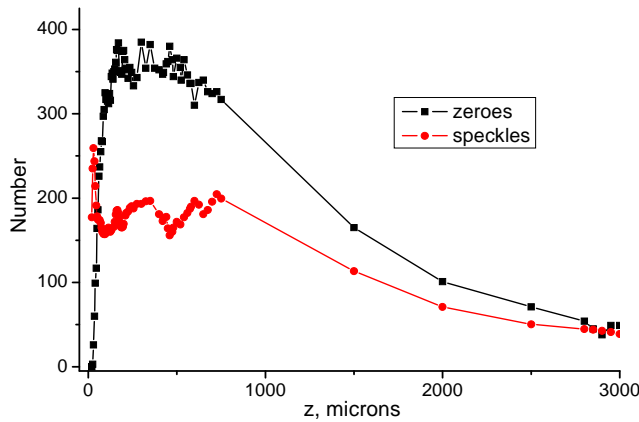

Fig. (21). The dependency of the number of amplitude zeroes in the registration plane determined for a model experiment, and the computed number of speckles found from the correlation length of intensity for a random rough surface with the interval of heights 2 μm.

For a fractal object with height intervals of 2 μm, the dependency of the number of speckles in the registration zone within an area of $40\text{x}40$ μm^2 are similar to the dependency obtained for a random rough surface (cf. Fig. **22**).
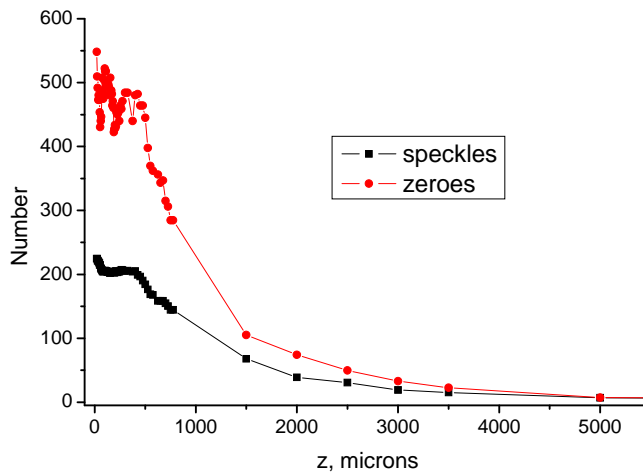

Fig. (22). The dependency of the number of amplitude zeroes in the registration plane determined in a model experiment and the computed number of speckles found from the intensity correlation

length for a fractal rough surface with the interval of heights equal to 2 μm.

The results of determination of the maximal number of phase singularities, N_{max}, and the maximal number of speckles estimated from the intensity distribution, N_i, for random rough surfaces with the intervals of heights h_{max} from 5 to $100\,\mu\text{m}$ for a field area of $10\text{x}10$ μm^2 are presented in Table **1**. One observes the correlation between the maximal number of phase singularities and the maximal number of speckles, in correspondence with the results presented in Fig. (**21**).

Table 1.   Determination of the Coordinates of Phase Singularities of a Field

h_{max}	l_I	N_{max}	N_i
5	0.47	65	36
10	0.3	144	89
20	0.215	280	172
30	0.18	361	246
50	0.17	432	275
100	0.17	451	275

Using position-sensitive detectors and modern computer techniques facilitates an experimental algorithm for determining the coordinates of phase singularities for optical fields. This technique consists in the determination of the intensity correlation function for local areas of size several pixels (minimum two), followed by computation of the ratio of their correlation lengths, and pixel-by-pixel connection of these parameters for the entire field.

The transverse correlation functions of a field and intensity can be determined experimentally. Correlation functions of a local field are determined for areas that are much smaller than the integral correlation length of the entire field. This means that the number of amplitude zeroes within one analyzed area can not exceed unity.

If an amplitude zero is absent, then the correlation lengths for intensity and for the field are equal. When an amplitude zero is present, then the correlation lengths of amplitude and intensity for this area are considerably different. This is the criterion for estimation of the presence of an amplitude zero within the analyzed area of the field.

The experimental steps for determining the coordinate distribution of phase singularities in the field are:

- the intensity distribution is registered by a CCD-camera;

- the maximal and minimal magnitudes of intensity of the resulting field are registered for shifts setting at the transverse shift interferometer – 1, 2, 3, …, N pixels;

- the intensity- and field correlation functions for local areas of size *N*x*N* pixels are computed with step size of one pixel;

- the ratio of the correlation lengths being less than 0.8 means that an amplitude zero is present within the analyzed area.

Let us consider the procedure for determining the coordinates of amplitude zeroes by analyzing the magnitudes of the correlation lengths of intensity and a field for local areas of a field.

The correlation function and coherence function for the field are computed for each pixel with coordinates (x, y) for specified shifts $0 \leq k \leq 3$.

The intensity correlation function is determined by the following equation:

$$F_{cor}\left(l\right)_{x,y} = \frac{\sum_{k}\left(I_{x+k,y+k} \times I_{x+k+l,y+k}\right)}{\sum_{k}I_{x+k,y+k} \times \sum_{k}I_{x+k+l,y+k}},$$

where $I_{x,y}$ is the intensity at (x, y). Further, one finds a half-width of the corresponding intensity correlation function:

$$R_{cor}\left(x, y\right) = \left| \frac{k - \dfrac{0.5 - F_{cor}\left(k\right)_{x,y}}{F_{cor}\left(k-1\right)_{x,y} - 0.5}}{1 + \dfrac{0.5 - F_{cor}\left(k\right)_{x,y}}{F_{cor}\left(k-1\right)_{x,y} - 0.5}} \right|.$$

For the same pixel as for the initial point one writes the minimal and maximal magnitudes of intensity, $I_{\min}\left(x, y\right)$ and $I_{\max}\left(x, y\right)$ resulting from interference of the field of this pixel with one of the adjacent pixel k (for the transverse shifts setting at the shift interferometer – 1, 2, 3,.., *N* pixels).

One obtains the transverse coherence function for the next three pixels. Then, one finds the coherence function by dividing the difference of $I_{\min}\left(x, y\right)$ and $I_{\max}\left(x, y\right)$ by their sum:

$$F_{coh}\left(l\right)_{x,y} = \sum_{k}\frac{I_{\max}\left(x+k+l, y+k\right) - I_{\min}\left(x+k+l, y+k\right)}{I_{\max}\left(x+k+l, y+k\right) + I_{\min}\left(x+k+l, y+k\right)}.$$

Further, one determines the half-width of the obtained function:

$$R_{coh}\left(x, y\right) = \left| \frac{k - \dfrac{0.5 - F_{coh}\left(k\right)_{x,y}}{F_{coh}\left(k-1\right)_{x,y} - 0.5}}{1 + \dfrac{0.5 - F_{coh}\left(k\right)_{x,y}}{F_{coh}\left(k-1\right)_{x,y} - 0.5}} \right|.$$

Estimating the ratio of the correlation length of intensity, $R_{cor}\left(x, y\right)$, to the correlation length of a field, $R_{coh}\left(x, y\right)$, one obtains a pixel-by-pixel distribution of the phase singularities of the field.

The intensity distribution of a field, including the coordinates of phase singularities determined from the behaviour of the local correlation length of field and intensity, is presented in Fig. (**23**).
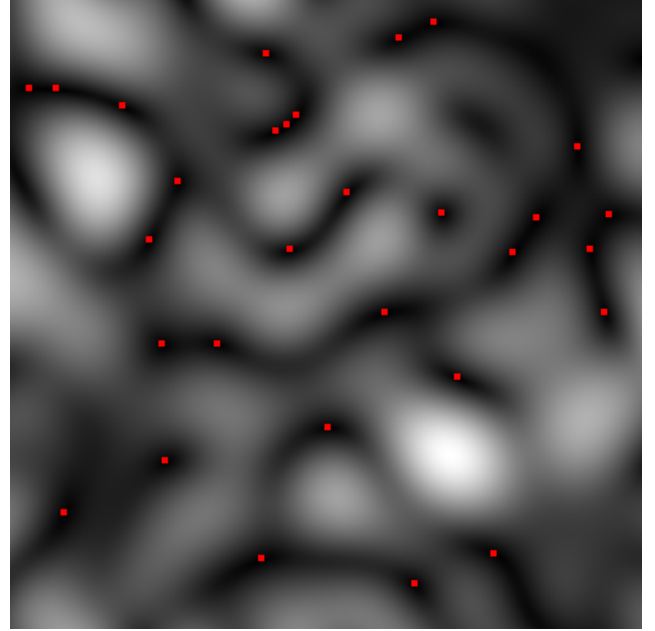

Fig. (23). Intensity distribution of a field with the coordinates of phase singularities determined from the behaviour of local correlation length of field and intensity.

CONCLUSIONS

The results of studying the peculiarities of the behaviour of amplitude zeros for fields scattered by fractal and random surfaces have been presented. It has been shown that the phase singularity lines are continuous lines, which in practice are not self-closing. Moreover, it has been shown that the phase singularity lines in the field scattered at fractal surfaces properties possess fractal properties; the phase singularity lines in the field scattered off non-fractal surfaces do not possess such properties. The optical correlation technique for diagnostics of phase singularities for complex speckle fields by comparing the correlation lengths of amplitude and intensity of the local fields has been proposed.

REFERENCES

[1] Goldfischer LI. Autocorrelation function and power spectral density of laser-produced speckle patterns. J Opt Soc Am 1965; 55: 247-52.

[2] Nye JF, Berry M. Dislocations in wave trains. Proc R Soc Lond 1974; A 336: 165-90.

[3] Nye JF. The Motion and structure of dislocations in wave fronts. Proc R Soc Lond 1981; A 378: 219-39.

[4] Baranova NB, Zeldovich B Ya. Wavefront dislocations and amplitude zeroes. Zhurnal Eksperimentalnoi Theoreticheskoi Fiziki 1981; 80: 1789-97.

[5] Baranova NB, Zeldovich B Ya, Mamayev AV, Pilipetsky NF, Shkunov VV. Investigation of wavefront dislocations density in the light field. JETP 1982; 83: 1702-10.

[6]   Baranova NB, Mamayev AV, Pilipetsky NF, Shkunov VV, Zeldovich B Ya. Wavefront dislocations: topological limitations for adaptive systems with phase conjugation. J Opt Soc Am 1983; 73: 525-28.

[7]   Angelsky OV, Maksimyak PP, Hanson SG. The Use of Optical-Correlation Techniques for Characterizing Scattering Object and Media. Bellingham: SPIE Press PM71 1999.

[8]   Angelsky OV, Maksimyak PP, Ryukhtin VV, Hanson SG. New feasibilities for characterizing rough surfaces by optical-correlation techniques. Appl Opt 2001; 40: 5693-707.

[9]   Angelsky OV, Maksimyak PP, Burkovets DN, Hanson SG. Applicability of the singular-optics concept for diagnostics of random and fractal rough surfaces. Appl Opt 2003; 42: 4529-40.

[10]   Voss RF. Random fractal forgeries. In: Earnshaw RA, Ed. Fundamental Algorithms in Computer Graphics, Berlin, Springer-Verlag 1985: 805-35.

[11]   Rytov SM, Kravtsov Yu A, Tatarsky VI. Principles of Statistical Radiophysics. Berlin: Springer Verlag 1989.

[12]   Goodman JW. Introduction to Fourier Optics. San Francisco, New York, St. Louis, Toronto, London, Sidney: McGraw-Hill Book Company 1968.

[13]   Nye JF. Natural focusing and fine structure of light. Bristol and Philadelphia: Institute of Physics Publishing 1999.

[14]   Freund I. Optical vortex trajectories, Opt Comm 2000; 181: 19-33.

[15]   Rozas D, Law CT, Swartzlander GA. Propagation dynamics of optical vortices. J Opt Soc Am B 1997; 14: 3054-65.

[16]   Rozas D, Sacks ZS, Swartzlander GA. Experimental observation of fluidlike motion of optical vortices. Phys Rev Lett 1997; 79: 3399-402.

[17]   Berry MV, Dennis MR. Knotted and linked phase singularities in monochromatic waves. Proc R Soc Lond 2001; A457: 2251-63.

[18]   O'Holleran, Dennis MR, Padgett MJ. Illustrations of optical vortices in three dimensions. J Eur Opt Soc Rap Public 2006; 1: 06008.

[19]   Berry M, Hannay J. Topography of random surfaces. Nature 1978; 273: 573.

[20]   Mandelbrot BB. The Fractal Geometry of Nature. San Francisco: W.H. Freeman 1984.

[21]   Strinadko MT, Tymochko BM, Dominikov NN. On transformation of speckle pattern with imposing reference wave. Opt Spectrosc 1991; 70: 416-20.

[22]   Angelsky OV, Strinadko MT, Timochko BM, Dominikov NN. Laboratory experiment concerning holographic recording of distant objects. Pure Appl Opt 1995; 4: 55-60.